Journal of Materials Chemistry A

Accepted Manuscript

ROYAL SOCIETY OF CHEMISTRY

www.rsc.org/materialsA

Journal Name

ARTICLE

Selective Photocatalytic N_2 Fixation Dependent on the g-C_3N_4 Induced by Nitrogen Vacancies

Received 00th January 20xx,
Accepted 00th January 20xx

DOI: 10.1039/x0xx00000x

www.rsc.org/

Guohui Dong*[a], Wingkei Ho[b], and Chuanyi Wang*[a]

Photoreduction of N_2 is among the most interesting and challenging methods for N_2 fixation under mild conditions. In this study, we determined that nitrogen vacancies (NVs) could endow graphitic carbon nitride (g-C_3N_4) with the photocatalytic N_2 fixation ability. Photocatalytic N_2 fixation induced by NVs is free from the interference of other gases. The reason is that NVs could selectively adsorb and activate N_2 because NVs have the same shape and size as the nitrogen atom in N_2. In addition to this, NVs could also improve many other properties of g-C_3N_4 to support photocatalytic N_2 fixation. These new findings could elucidate the design of efficient photocatalysts for photocatalytic N_2 fixation.

Introduction

Nitrogen is an essential building element of life on Earth. However, molecular nitrogen is nutritionally unavailable because nitrogen molecules are held together by a strong N≡N triple bond. Moreover, most plants can only take up nitrogen in the forms of ammonium ion (NH_4^+) and nitrate ion (NO_3^-) despite its abundance of 78% in the atmosphere.[1–3] Rainfall and lightning could bring a certain amount of nitrogen in the atmosphere into the soil. Biochemical N_2 fixation within the soil, which occurs with the help of specialized microorganisms, such as bacteria, actinomycetes, and cyanobacteria, contributes to most of the natural nitrogen nutrient.[4–6] However, these natural nitrogen sources do not satisfy the increased demand of modern agriculture. The Haber–Bosch process, a well-known large-scale, continuous-flow, high-pressure, and high-temperature artificial nitrogen fixation technology, produces 500 million tons of artificial nitrogen fertilizer per year, which is responsible for sustaining one third of the Earth's population.[7–10] However, this process consumes approximately 1% to 2% of the annual energy supply of the world and results in various deleterious environmental consequences. Therefore, artificial nitrogen fixation under mild conditions is among the most important and challenging topics in scientific and technological fields.

Photocatalytic N_2 fixation is one of the most interesting and challenging methods for artificial nitrogen fixation under mild conditions because this strategy uses renewable and sufficient solar energy as the driving force. The first study on photocatalytic N_2 fixation was reported by Schrauzer and Guth in 1977. They determined that iron-doped TiO_2 could photocatalytically reduce molecular nitrogen (N_2) to ammonia under UV light irradiation.[11] Afterward, Radford and Francis investigated photocatalytic N_2 fixation on iron-doped anatase and rutile in 1983. Their results showed that doped anatase was more active than doped rutile.[12] Based on previous studies, $Fe_2Ti_2O_7$ and $SrTiO_3$ were synthesized, and it was reported that they exhibited remarkable N_2 photofixation ability under visible light irradiation.[13, 14] In previous publications, the photocatalysts used for N_2 photofixation focused only on titanium oxide and titanate. However, many other studies have shown that released nanomaterials, such as titanium oxide and titanate, exhibit toxic effects on organisms.[15, 16] In addition, the production rates of ammonia are very low (only approximately 0 μM/h to 9 μM/h) in most of the previous photocatalytic N_2 fixation processes. The production rate of ammonia decreases after a few hours of light irradiation because the ammonia produced could be further oxidized by photogenerated holes. These disadvantages limit the development and practical use of photocatalytic N_2 fixation. Designing new photocatalysts that have a strong ability to selectively photocatalyze N_2 fixation is not only important but also a challenge in the promotion of the development of photocatalytic N_2 fixation.

Recently, Li and his coworkers investigated the photocatalytic N_2 fixation on BiOBr nanosheets. They observed that the photocatalytic N_2 fixation activity of BiOBr could significantly improve by introducing several oxygen vacancies (OVs).[17] OVs could activate N_2 and significantly promote interfacial electron transfer. Their results give us an inspiration that nitrogen vacancies (NVs) may be more effective for photocatalytic N_2 fixation than OVs. First, NVs have the same shape and size as the nitrogen atom in N_2. Thus,

[a] Laboratory of Environmental Sciences and Technology, Xinjiang Technical Institute of Physics & Chemistry, and Key Laboratory of Functional Materials and Devices for Special Environments, Chinese Academy of Sciences, Urumqi 830011, China.
[b] Department of Science and Environmental Studies and Centre for Education in Environmental Sustainability, The Hong Kong Institute of Education, Tai Po, N.T. Hong Kong, People's Republic of China.
* To whom correspondence should be addressed. E-mail: donggh@ms.xjb.ac.cn. Phone: +86-15199153105

Electronic Supplementary Information (ESI) available: [Experimental details of simulation, isotopic labelling experiments, and photocurrent experiments; mass spectra; TEM images; adsorption models; photocatalytic N_2 fixation in mixed gas; the generation of CO and the generation of CH_4]. See DOI: 10.1039/x0xx00000x

NV-containing material is like the N_2-imprinted polymer. As well as we known, molecular-imprinted polymer is an emerging material for selective recognition. Therefore, NVs may be used as excellent adsorbents and activators for N_2.[18] Second, NVs as defects can trap photogenerated electrons to inhibit the recombination of photogenerated carriers.[19] To validate these considerations, we select graphitic carbon nitride (g-C_3N_4) as the photocatalyst for the photocatalytic N_2 fixation experiments. This is because g-C_3N_4 has visible light response, and NVs could be introduced into the framework of g-C_3N_4 by using a simple method.[20, 21] In this study, we report for the first time that NV-incorporated g-C_3N_4 (V-g-C_3N_4) can selectively photoreduce N_2 and free from the interference of other gases. A series of experiments is designed to investigate the relationship between NVs and N_2 photofixation ability of g-C_3N_4. The reasons for the selective photocatalytic N_2 fixation are analyzed in detail.

Experimental Section

Preparation of the Catalysts. All chemicals used were analytical-grade reagents without further purification. g-C_3N_4 was synthesized by directly heating melamine based on previous reports.[19,20] Typically, melamine was placed in a covered crucible and heated to 500 °C for 2 h with a heating rate of 20 °C/min, followed by further heat treatment at 520 °C for 2 h. V-g-C_3N_4 was synthesized by calcining as-prepared g-C_3N_4 in a tube furnace at 520 °C under N_2 flow for 2 h.

Characterization of the Photocatalysts. Powder X-ray diffraction (XRD) patterns were recorded on a Bruker D8 Advance diffractometer with monochromatized Cu Kα radiation (λ = 1.5418 Å). X-ray photoelectron spectroscopy (XPS) measurements were conducted in a VG Scientific ESCALAB Mark II spectrometer equipped with two ultrahigh vacuum chambers. All the binding energies were calibrated to the C 1s peak at 284.6 eV of the surface adventitious carbon. The carbon-to-nitrogen (C/N) ratio of the samples was determined by elemental analysis (EA; Vario EL III CHNSO). Electron spin resonance (ESR) signals were recorded on a Bruker ESR A300 spectrometer at room temperature (298 K). The nitrogen adsorption and desorption isotherms at 77 K were measured using the Micrometrics ASAP2020 system after samples were vacuum-dried at 180 °C overnight. UV–vis diffuse reflectance spectra of samples were obtained using an UV–vis spectrometer (Shimadzu UV-2550).

Photocatalytic N_2 Fixation Experiments. The photocatalytic N_2 fixation experiments were conducted in a 100 mL reaction cell with an external cooling water jacket at ambient temperature and atmospheric pressure. A 300 W Xe lamp through an UV cutoff filter (λ > 420 nm) was used as the light source. In a typical experiment, 50 mg of photocatalyst powder was suspended in 50 mL of aqueous solution containing 20% methanol (a type of photogenerated hole scavenger) in volume. N_2 (purity ⩾ 99.999%) was bubbled through this solution for 1 h in the dark to establish an adsorption–desorption balance and saturate the solution with N_2. Then, the reactor was sealed and shined with visible light (λ > 420 nm). During light irradiation, approximately 5 mL of the suspension was obtained from the reaction cell at given intervals for subsequent NH_4^+ concentration analysis.

NH_4^+ concentration analysis was conducted using Nessler's reagent method. First, 5 mL of the suspension was filtered through a 0.22 μm membrane filter and placed in a 10 mL sample tube. Then, 100 μL of the potassium sodium tartrate solution was added to the sample tube. After blending, 150 μL of Nessler's reagent was added to the same sample tube and mixed. Then, the mixture was left to stand for 10 min for full color processing. Finally, the concentration of NH_4^+ was tested using an UV–vis spectrophotometer (Shimadzu UV-2550) at λ = 425 nm.

Results and Discussion

XRD was used to characterize the phase structure of the final samples (Fig. 1a). The samples of g-C_3N_4 and V-g-C_3N_4 contained two peaks at approximately 13.0° and 27.4°, which matched well with the (100) and (002) crystal planes of g-C_3N_4. The (100) crystal plane was attributed to the in-planar repeating triazine unit. By contrast, the (002) crystal plane with a strong diffraction peak was related to the layer stacking of aromatic systems. The (100) peak of V-g-C_3N_4 samples became weaker and broader than that of g-C_3N_4 samples, corresponding with the decrease in the order degree of in-plane structural packing. This finding indicates that many defects may exist in the V-g-C_3N_4 framework. Moreover, the peak at 27.4° of V-g-C_3N_4 shifts toward a larger 2θ value, corresponding to a decrease in the interlayer stacking distance, which may be due to the reduction in the repulsion between the interlayers caused by defects. In addition to XRD analysis, ESR could also prove the formation of defects. Fig. 1b shows that g-C_3N_4 exhibits a Lorentzian line originating from the unpaired electrons on the carbon atoms of the aromatic rings. This Lorentzian line was considerably enhanced after heat treatment with nitrogen gas because the formation of defects increased the number of unpaired electrons.

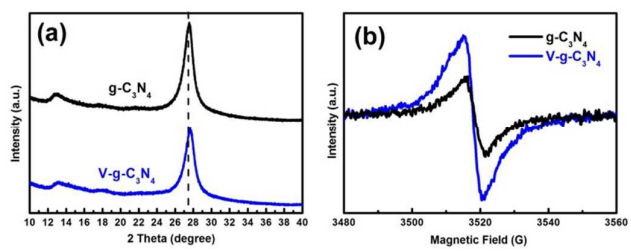

Fig. 1 XRD patterns (a) and ESR spectra (b) of g-C_3N_4 and V-g-C_3N_4.

EA was used to determine the C/N molar ratio in the final samples and to determine the type of defects formed in the V-g-C_3N_4 framework (Fig. 2a). The C/N molar ratio of V-g-C_3N_4 was 0.75, which was lower than that of g-C_3N_4 (0.81). This finding indicates that the defects formed in the V-g-C_3N_4 framework were NVs. XPS was further used to investigate the chemical compositions of the final samples (Fig. 2b and 2c). The high-resolution XPS spectrum of N 1s could be fitted with three peaks (Fig. 2b). Based on previous reports, the main peaks at 398.4 and 400.7 eV can be attributed to the C–N–C groups and tertiary nitrogen N–C_3 groups, respectively.

Journal Name

ARTICLE

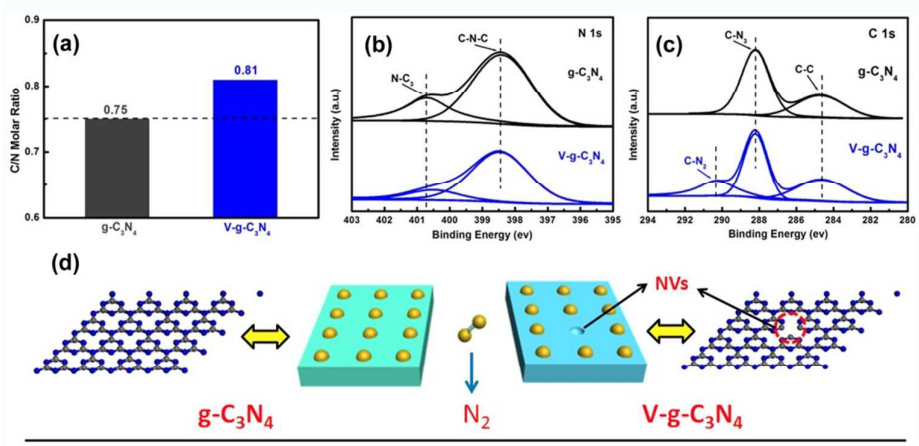

Fig. 2 C/N molar ratio in the g-C_3N_4 and V-g-C_3N_4 (a); high-resolution XPS spectra of N 1s of g-C_3N_4 and V-g-C_3N_4 (b); high-resolution XPS spectra of C 1s of g-C_3N_4 and V-g-C_3N_4 (c); schematics of g-C_3N_4 and V-g-C_3N_4 (d).

Notably, the N 1s peak from N–C_3 was significantly weakened. As such, the peak–area ratio of N–C_3 to C–N–C decreased from 3.25 to 0.76, clearly indicating that NVs were mainly located at the tertiary nitrogen lattice sites. In addition, the high-resolution XPS peaks of C 1s of g-C_3N_4 can be fitted with two peaks at binding energies of 284.6 and 288.2 eV, which were ascribed to the tertiary carbon C–N_3 and C–C (arising from the adventitious carbon) groups, respectively. However, in addition to the C 1s peaks at 284.6 and 288.2 eV, a new peak at a high binding energy of 290.3 eV appears in the high-resolution XPS spectra of V-g-C_3N_4 (Fig. 2c). This peak is attributed to the two-coordinated carbon (N–C–N) formed by the disappearance of three-coordinated nitrogen, thereby confirming the generation of NVs (Fig. 2d).

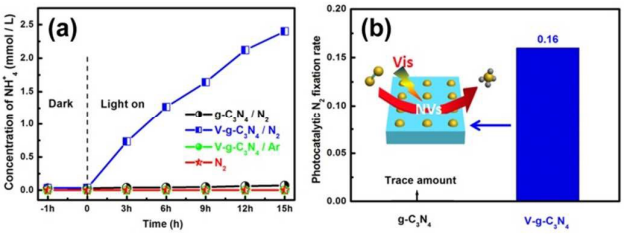

Fig. 3 The concentration of generated NH_4^+ in different systems (a); photocatalytic N_2 fixation rate of g-C_3N_4 and V-g-C_3N_4 (b).

The photocatalytic activities of the final samples were measured in photocatalytic N_2 fixation experiments (Fig. 3a). Control experiments showed that NH_4^+ cannot be detected in the absence of any one of three facts, namely, photocatalyst, N_2, and visible light irradiation. This finding indicates that the photocatalyst, N_2, and visible light were necessary for the present photocatalytic N_2 fixation. After 15 h of visible light irradiation, no significant amount of NH_4^+ was detected in the case of g-C_3N_4, whereas V-g-C_3N_4 could generate 2.4 mM of NH_4^+ in the N_2 atmosphere. The photocatalytic N_2 fixation rate was 1.24 mmol/h per 1 g of V-g-C_3N_4 (Fig. 3b). Moreover, when nitrogen gas was replaced by high-purity argon gas (purity $\geqslant$ 99.999%), the photocatalytic N_2 fixation activity of V-g-C_3N_4 disappeared. Evidently, V-g-C_3N_4 exhibited higher reactivity in photocatalytic N_2 fixation, confirming the vital function of NVs in the photocatalytic N_2 fixation on g-C_3N_4.

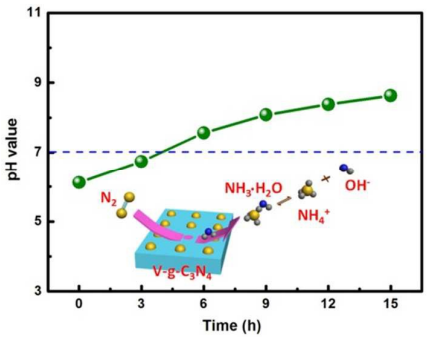

Fig. 4 The pH value change of the V-g-C_3N_4 suspension during the photocatalytic N_2 fixation process.

We analyze the pH value change of the V-g-C_3N_4 suspension during the photocatalytic N_2 fixation process to understand the photocatalytic N_2 fixation on V-g-C_3N_4. Before photocatalytic N_2 fixation, the pH value of the suspension is measured as 6.12. However, this pH value increased to 8.63 after 15 h of

photocatalytic N_2 fixation (Fig. 4) because the process requires a significant amount of H^+. In addition, N_2 was first reduced to NH_3, which consumes H^+, and was changed to NH_4^+. Although protons may be supplied by the oxidation reaction, the rate of proton consumption is greater than that of proton production. Therefore, the pH is increased in the process of photocatalytic N_2 fixation. The increase in pH value can be observed clearly from the following equations:

$$N_2 + 6H^+ + 6e^- \rightarrow 2NH_3 \quad (1)$$

$$NH_3 + H_2O \rightarrow NH_3{\cdot}H_2O \leftrightharpoons NH_4^+ + OH^- \quad (2)$$

We investigated the Rhodamine B (RhB, 5 mg/L) photooxidation of two samples under aerobic and anoxic conditions to verify the authenticity of photocatalytic N_2 fixation on V-g-C_3N_4. After visible light irradiation for 60 min under aerobic conditions, the photodegradation efficiencies of RhB over g-C_3N_4 and V-g-C_3N_4 were approximately 30% and 64%, respectively (Fig. 5a and 5b). When air was eliminated by purging with high-purity argon gas, the RhB photooxidation rate on g-C_3N_4 and V-g-C_3N_4 decreased significantly. This finding was not surprising because photooxidation requires the participation of molecular oxygen and/or molecular nitrogen for the capture of photogenerated electrons to inhibit the recombination between photogenerated holes and photogenerated electrons. To further clarify photoelectrons capturer of g-C_3N_4 and V-g-C_3N_4 in air, high-purity nitrogen gas and high-purity oxygen gas were selected as replacements for high-purity argon gas to eliminate air. When high-purity nitrogen gas was selected eliminate air, the photooxidation efficiency of RhB on V-g-C_3N_4 exhibited no significant change, whereas that on g-C_3N_4 significantly decreased. If air was eliminated by oxygen, the photooxidation efficiency of RhB on V-g-C_3N_4 significantly decreased, while that on g-C_3N_4 exhibited a slightly increase. These observations suggested that oxygen was the photoelectrons capturer of g-C_3N_4 in air, while nitrogen was the photoelectrons capturer of V-g-C_3N_4 in air. These observations were the evidence that N_2 could be reduced on V-g-C_3N_4. Therefore, we conclude that NVs endow g-C_3N_4 with the photocatalytic N_2 fixation ability.

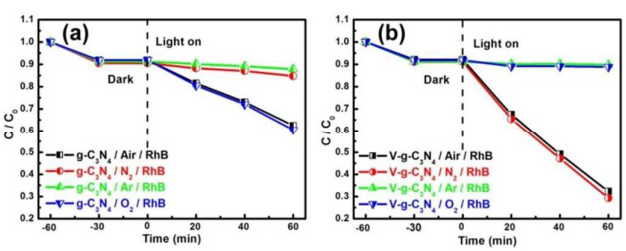

Fig. 5 The impact of N_2, Ar and O_2 on the RhB photooxidation ability of g-C_3N_4 (a) and V-g-C_3N_4 (b).

In order to further prove the authenticity of photocatalytic N_2 fixation on V-g-C_3N_4, the photocatalytic N_2 fixation under 15N-isotope-labeled N_2 (purity ⩾ 98.5%) was performed. Generated $15NH_4^+$ reacts with phenolic and hypochlorite to form 15N-labeled indophenol, which was analysed by LC-MS. It is important to note that a strong 15N-labeled indophenol anion mass spectroscopy signal presented at 199 m/z in LC-MS studies (Fig. S1, in the supporting information). The intensity of this signal relatively higher than that of 14N:15N natural abundance ratio. This observation further confirmed that N_2 was the source of generated ammonium ion in our experiment.

Photocatalytic N_2 fixation is a heterogeneous catalysis reaction. To our knowledge, adsorption is a necessary prerequisite of the heterogeneous catalysis reaction. Therefore, we compared the nitrogen gas physical adsorption ability of g-C_3N_4 and V-g-C_3N_4 to clarify the reasons for the excellent photocatalytic N_2 fixation activity of V-g-C_3N_4. Fig. 6a shows that the Brunauer–Emmett–Teller specific surface areas of g-C_3N_4 and V-g-C_3N_4 are 8.2 and 17.4 m^2/g, respectively. The N_2 adsorption amount of g-C_3N_4 and V-g-C_3N_4 at P/P0 = 0.986 are 30.9 and 75.1 cm^3/g, respectively, indicating that heat treatment with nitrogen gas increases the N_2 physical adsorption ability of the final product by 2.4 times. However, 2.4 times of N_2 physical adsorption on V-g-C_3N_4 were less than the countless times of photocatalytic N_2 fixation on V-g-C_3N_4. The excellent photocatalytic N_2 fixation activity of V-g-C_3N_4 is due not only to better N_2 physical adsorption ability but also to other more important factors related to the NVs.

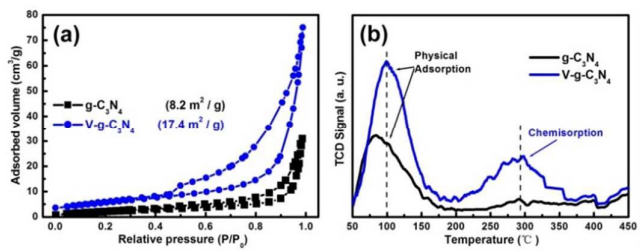

Fig. 6 N_2 adsorption-desorption isotherms (a) and TPD spectra (b) of the as-prepared g-C_3N_4 and V-g-C_3N_4.

As the chemical adsorption sites are regarded as reaction centers capable of activating N_2, chemisorption is an essential step in photocatalytic N_2 fixation. Temperature-programmed desorption (TPD) investigations have been conducted to understand N_2 chemisorption on the surface of g-C_3N_4 and V-g-C_3N_4. In Fig. 6b, we compared the results of TPD studies of N_2 on g-C_3N_4 and V-g-C3N4. We clearly observed two adsorbed N_2 species in V-g-C_3N_4 catalyst and only one adsorbed N_2 species in g-C_3N_4. The peak of g-C_3N_4 at approximately 100 °C, which was related to physical adsorption, is weaker than that of V-g-C_3N_4. This finding is in agreement with results in previous studies on N_2 adsorption–desorption isotherms. Moreover, the peak at 295 °C, which was related to the strong chemisorption species of N_2, was observed for V-g-C_3N_4, but not for g-C_3N_4. This finding indicated that NVs could introduce many chemical adsorption sites on the surface of V-g-C_3N_4. Because chemisorption is usually associated with the activation, these chemical adsorption sites will activate N_2 and endow V-g-C_3N_4 with the photocatalytic N_2 fixation ability.

Considering that NVs have the same shape and size as the nitrogen atom in N_2, we believe that NVs on the V-g-C_3N_4 surface are the chemical adsorption sites of N_2. The surface of V-g-C_3N_4 was loaded with palladium (Pd) through the photodeposition method to confirm this opinion. Given that

Journal Name

ARTICLE

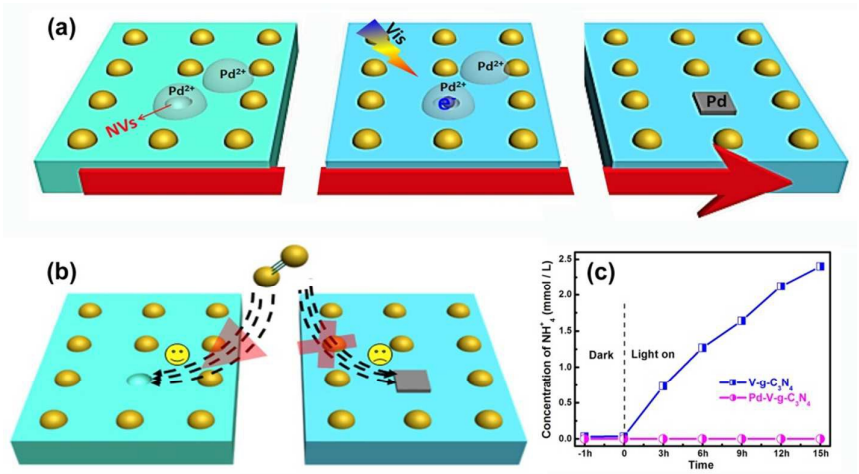

Fig. 7 Pd particles can be selectively deposited onto NVs (a); N_2 will not be adsorbed on the Pd particale because of the considerable work function (b); the loading of Pd onto V-g-C_3N_4 can completely suppress photocatalytic N_2 fixation (c).

photogenerated electrons are confined in the NVs, Pd particles can be selectively deposited onto NVs (Fig. 7a). Moreover, N_2 will not be adsorbed on the platinum group metals because of the considerable work function of these metals (Fig. 7b).[22] Therefore, when NVs are the chemical adsorption sites of N_2, the modification of Pd particles will block N_2 adsorption, thereby inhibiting N_2 photoreduction. Fig. 7c shows that the loading of Pd onto V-g-C_3N_4 (Fig. S2) can completely suppress photocatalytic N_2 fixation, confirming that N_2 was mainly adsorbed on the surface NVs of V-g-C_3N_4.

To further confirm that N_2 was mainly adsorbed on the NVs and activated by NVs, density functional theory (DFT) simulations were employed to investigate the interaction between N_2 molecule and V-g-C_3N_4 surface. Once the geometric structure of V-g-C_3N_4 was modelled, we optimized it with a N_2 molecular above the V-g-C_3N_4 surface. The optimized results indicated that N_2 molecule prefer adsorbing on the NVs. When N_2 molecule adsorbs on the NVs, two σ bonds between N_2 molecule and two nearest C atoms are formed (Fig. S3), confirming N_2 was mainly adsorbed on the NVs. After N_2 molecule combined with NVs, the coupling scheme of N_2 molecule changed as the bond length relaxed from 1.117 Å to 1.214 Å, proving that NVs could activate N_2.

Since NV-containing material is like the N_2-imprinted polymer, we believe that many other gases, such as oxygen and carbon dioxide, do not affect the photocatalytic N_2 fixation activity of V-g-C_3N_4. To test this hypothesis, N_2 was replaced by mixed gas (N_2, O_2 and CO_2 with the volume ratio of 1:1:1) in the photocatalytic N_2 fixation experiment. As shown in Fig. S4, the presence of O_2 and CO_2 does not affect the photocatalytic N_2 fixation activity of g-C_3N_4 and V-g-C_3N_4. This is evidence that the photocatalytic N_2 fixation activity of V-g-C_3N_4 is free from the interference of other gases. Besides the investigation of photocatalytic N_2 fixation activity, by products were also investigated to check if the N_2 fixation of V-g-C_3N_4 has selectivity. We firstly tested the H_2 generated in the process of photocatalytic N_2 fixation under the mixed gas condition. However, there were no any H_2 could be detected over both g-C_3N_4 and V-g-C_3N_4. Additionally, CO and CH_4 were also investigated. The tested results shown that CO and CH_4 could be detected in the reactor of g-C_3N_4, but not detected in the reactor of V-g-C_3N_4, indicating NVs could not transmit electrons from V-g-C_3N_4 to CO_2 (Fig. S5). Moreover, we used the 5,5-dimethyl-pyrroline N-oxide (DMPO) spin trapping ESR technique to measure $\cdot O_2^-$ generated during photocatalysis under mixed gas saturated conditions (Fig. 8a). Four characteristic peaks of DMPO-$\cdot O_2^-$ were evidently observed in methanolic suspensions of g-C_3N_4, while no peaks could

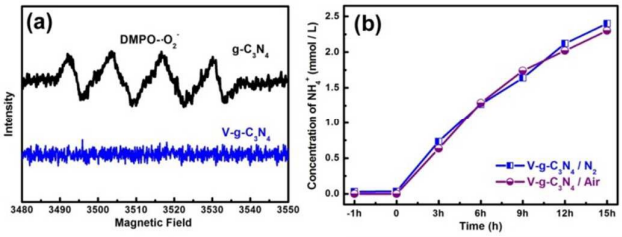

Fig. 8 5,5-dimethyl-pyrroline N-oxide (DMPO) spin trapping ESR technique to measure $\cdot O_2^-$ generated during photocatalysis under mixed gas saturated conditions (a); The replacement of N_2 with air does not change the photocatalytic N_2 fixation rate on V-g-C_3N_4 (b).

be observed in methanolic suspensions of V-g-C_3N_4, reflecting that electrons dose not be transferred from the surface of V-g-C_3N_4 to molecular oxygen. All these phenomena confirmed that NVs could selectively adsorb and reduce N_2 from many gases. Based on this result, it is reasonable to consider that V-g-C_3N_4 could directly photoreduce N_2 in the air atmosphere. To test this speculation, N_2 was replaced by air in the photocatalytic N_2 fixation experiment. The replacement of N_2 with air does not change the photocatalytic N_2 fixation rate on V-g-C_3N_4 (Fig. 8b). Therefore, V-g-C_3N_4 is more efficient and practical than previous photocatalysts in photocatalytic N_2 fixation because V-g-C_3N_4 is free from the interference of other gases.

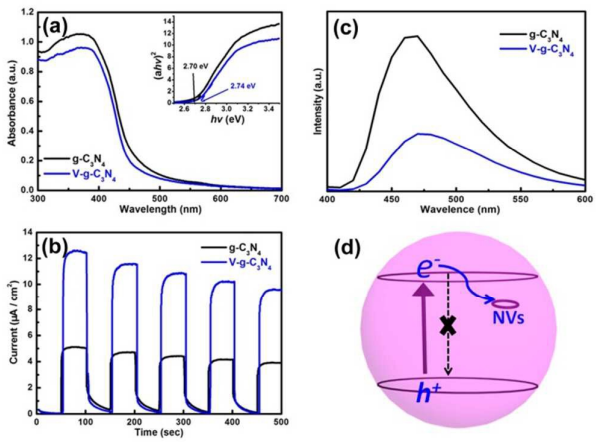

Fig. 9 The UV–vis diffuse reflectance spectra of g-C_3N_4 and V-g-C_3N_4 (a); the photocurrent generated on V-g-C_3N_4 was significantly higher than that on g-C_3N_4 (b); photoluminescence (PL) spectra are used to investigate the recombination and separation of photogenerated electrons and holes in the g-C_3N_4 and V-g-C_3N_4 samples (c). NVs can act as electron trappers to improve carrier separation (d)

In addition to adsorption and activation, the redox ability and photoelectrons strongly affect the photoreduction activity of a semiconductor. The UV–vis diffuse reflectance spectra of the samples are recorded (Fig. 9a). DRS analysis reveals that g-C_3N_4 and V-g-C_3N_4 absorbs visible light in the range of 400 nm to 700 nm. The band gap energy of V-g-C_3N_4 is approximately 2.74 eV, which was slightly larger than that of g-C_3N_4 (2.70 eV). We believe that the enlarged band gaps of V-g-C_3N_4 are attributed to quantum confinement effect (QCE) because of the introduction of NVs. Since QCE could increase the bandgap by oppositely shifting valence and conduction band edges, the conduction band of V-g-C_3N_4 should possess more powerful photoreduction ability than that of g-C_3N_4. However, the enlarged band gap would reduce the visible light use efficiency and make the electronic excitation of semiconductor more difficult under visible light. Normally, V-g-C_3N_4 with enlarged band gap would produce a lower photocurrent than g-C_3N_4. However, we observed the photocurrent generated on V-g-C_3N_4 was significantly higher than that on g-C_3N_4 (Fig. 9b). Photocurrent relies on the amount of photoelectrons transferred from the semiconductor to the fluorine-doped tin oxide (FTO) glass substrate. Therefore, higher photocurrent implies that the NVs inhibit the recombination of the photogenerated carriers and eventually produce more photoelectrons. Then, photoluminescence (PL) spectra are used to investigate the recombination and separation of photogenerated electrons and holes in the g-C_3N_4 and V-g-C_3N_4 samples (Fig. 9c). The emission peak that appears at approximately 455 nm was attributed to the direct electron and hole recombination of band transition. Compared with g-C_3N_4, V-g-C_3N_4 has a weaker emission peak, confirming that NVs can act as electron trappers to improve carrier separation (Fig. 9d). Powerful photoreduction activity and carrier separation efficiency further improve the photocatalytic N_2 fixation activity of V-g-C_3N_4.

The photogenerated electrons that arrive at the surface of g-C_3N_4 or are trapped by the NVs of V-g-C_3N_4 should be immediately transferred from the semiconductors to the adsorbed N_2 to trigger photocatalytic N_2 fixation. Li and his coworkers revealed that OVs promote interfacial charge transfer from BiOBr nanosheets to N_2. We hypothesized that NVs also promote photogenerated electron transfer from g-C_3N_4 to adsorbed N_2. Photocurrent measurement and PL spectra are further used to collect information on the effects of NVs on interfacial electron transformation to test this hypothesis. Under N_2 atmosphere, the photocurrent generated on g-C_3N_4 electrode is unchanged with irradiation time during the entire irradiation period. However, the photocurrent density of V-g-C_3N_4 under N_2 atmosphere gradually decreases with irradiation time, as shown in Fig. 10a. Photocurrent decay mainly occurs because of the competition between N_2 and FTO glass for trapped electrons, confirming that NVs promote photogenerated electron transfer from g-C_3N_4 to adsorbed N_2. Fig. 10b shows the PL spectra of V-g-C_3N_4 under Ar and N_2 atmospheres. Under N_2 atmosphere, the intensity of the emission peak caused by the combination of electrons and holes has been significantly reduced compared with that under Ar atmosphere. By contrast, no difference between the PL spectra of g-C_3N_4 under the N_2 and Ar atmosphere is observed (Fig. 10b), further confirming that NVs promote photogenerated electron transfer from g-C_3N_4 to adsorbed N_2.

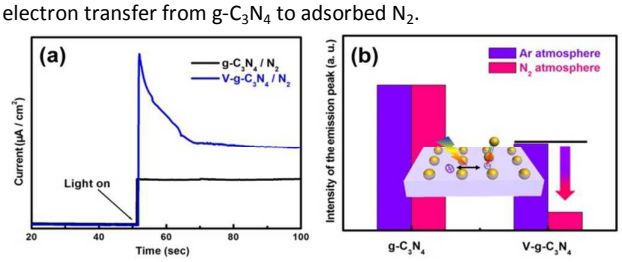

Fig. 10 The photocurrent density of g-C_3N_4 and V-g-C_3N_4 under N_2 atmosphere (a); the intensity of PL spectra of g-C_3N_4 and V-g-C_3N_4 under Ar and N_2 atmospheres, respectively (b).

NVs endow g-C_3N_4 with the photocatalytic N_2 fixation ability for three reasons. First, NVs selective adsorb and activate N_2 because NVs have the same shape and size as the nitrogen atom in N_2. Second, NVs effectively improve the separation efficiency of photogenerated carriers and generate more photoelectrons. Third, NVs promote photogenerated electron

transfer from g-C_3N_4 to adsorbed N_2. All three reasons make photocatalytic N_2 fixation on the surface of V-g-C_3N_4 easier.

Conclusions

We successfully synthesized V-g-C_3N_4 by heat treatment with nitrogen gas. In the photocatalysis experiments, we observed that NVs could endow g-C_3N_4 with the photocatalytic N_2 fixation ability. NVs selectively adsorbed and activated N_2 because NVs have the same shape and size as the nitrogen atom in N_2. The photocatalytic N_2 fixation process was free from the interference of other gases because of selective adsorption and activation. In addition to this advantage, NVs also improved the separation efficiency of photogenerated carriers and the electron transfer from g-C_3N_4 to adsorbed N_2. This study is the first to report on how NVs affect the reactivity of semiconductors on N_2 photofixation. The new findings could elucidate the design of efficient photocatalysts for selective photocatalytic N_2 fixation.

Acknowledgements

This work was supported by National Science Foundation of China (Grants 21473248) and scientific research start-up funds for postdoctor (Y55P411601). We thank Dr Ziyan zhong (WHU, China) and Dr Dapeng Sun (CCNU, China) for help in TPD and BET measurments, and Prof. Wingkei Ho (HKIEd, Hong Kong) for language polish.

Notes and references

1 J. Chatt, J. R. Dilworth and R. L. Richards, *Chem. Rev.* 1978, **78,** 589-625.
2 J. A. Brandes, A. H. Devol and C. Deutsch, *Chem. Rev.* 2007, **107,** 577-589.
3 R. J. Haynes and K. M. Goh, *Biol. Rev.* 1978, **53,** 465-510.
4 H. Tanaka, H. Mori, H. Seino, M. Hidai, Y. Mizobe and K. Yoshizawa, *J. Am. Chem. Soc.* 2008, **130,** 9037-9047.
5 G. D. Werner, W. K. Cornwell, J. I. Sprent, J. Kattge and E. T. Kiers, *Nat. Commun.* 2014, **5,** 4087.
6 B. M. Hoffman, D. Lukoyanov, Z. Y. Yang, D. R. Dean and L. C. Seefeldt, *Chem. Rev.* 2014, **114,** 4041-4062.
7 (a) M. D. Fryzuk, *Science* 2013, **340,** 1530-1531; (b) T. Kandemir, M. E. Schuster, A. Senyshyn, M. Behrens and R. Schlogl, *Angew. Chem. Int. Ed.* 2013, **52,** 12723-12726.
8 (a) T. Shima, S. W. Hu, G. Luo, X. H. Kang, Y. Luo and Z. M. Hou, *Science* 2013, **340,** 1549-1552; (b) C. Rebreyend and B. D. Bruin, *Angew. Chem. Int. Ed.* 2015, **54,** 42-44.
9 (a) M. S. Scheibel and S. Schneider, *Angew. Chem. Int. Ed.* 2012, **51,** 4529-4531; (b) B. Yang, R. Burch, C. Hardacre, G. Headdock and P. Hu, *ACS Catal.,* 2014, **4,** 182-186.
10 (a) J. W. Erisman, M. A. Sutton, J. Galloway, Z. Klimont and W. Winiwarter, *Nature Geosci.* 2008, **1,** 636-639. (b) J. J. Scepaniak, C. S. Vogel, M. M. Khusniyarov, F. W. Heinemann, K. Meyer and J. M. Smith, *Science* 2011, **331,** 1049-1052.
11 G. N. Schrauzer and T. D. Guth, *J. Am. Chem. Soc.* 1977, **99,** 7189-7193.
12 P. P. Radford and C. G. Francis, *J. Chem. SOC., Chem. Commun.,* 1983, **871,** 1520-1521.
13 O. Rusina, A. Eremenko, G. Frank, H. P. Strunk and H. Kisch, *Angew. Chem. Int. Ed.* 2001, **40,** 3993-3995.
14 (a) T. Oshikiri, K. Ueno, H. Misawa, *Angew. Chem. Int. Ed.* 2014, **126,** 9960-9963. (b) O. Rusina, O. Linnik, A. Eremenko and H. P. Strunk, *Chem. Eur. J.* 2003, **9,** 561-565.
15 (a) P. R. Gil, G. Oberdorster, A. Elder, V. Puntes and W. J. Parak, *ACS Nano,* 2010, **10,** 5527-5531; (b) S. C. Kim and D. K. Lee, *Microchem. J.* 2005, **80,** 227-232.
16 V. Aruoja, H. C. Dubourguier, K. Kasemets and A. Kahru, *Sci. Total Environ.* 2009, **407,** 1461-1468.
17 H. Li, J. Shang, Z. H. Ai and L. Z. Zhang, *J. Am. Chem. Soc.* 2015, **137,** 6393-6399.
18 (a) L. Ye and K. Mosbach, *J. Am. Chem. Soc.* 2001, **123,** 2901-2902; (b) M. Subat, A. S. Borovik and B. Konig, *J. Am. Chem. Soc.* 2004, **126,** 3185-3190.
19 (a) G. H. Dong and L. Z. Zhang, *J. Mater. Chem.* 2012, **22,** 1160-1166; (b) Q. L. Tay, P. Kanhere, C. F. Ng, S. Chen, S. Chakraborty, A. C. H. Huan, T. C. Sum, R. Ahuja and Z. Chen, *Chem. Mater.* 2015, **27,** 4930-4933.
20 (a) X. C. Wang, K. Maeda, A. Thomas, K. Takanabe, G. Xin, J. M. Carlsson, K. Domen and M. A. Antonietti, *Nat. Mater.* 2009, **8,** 76-80; (b) Y. Wang, Y. Di, M. Antonietti, H. R. Li, X. F. Chen and X. C. Wang, *Chem. Mater.* 2010, **22,** 5119-5121.
21 P. Niu, G. Liu and H. M. Cheng, *J. Phys. Chem. C,* 2012, **116,** 11013-11018.
22 (a) B. M. W. Trapnell, *Proc. R. Soc.* 1953, **A218,** 566-577; (b) Z. M. Liu, Y. Zhou, F. Solymosi and J. M. White, *Surf. Sci.* 1991, **245,** 289-304.

Table of contents

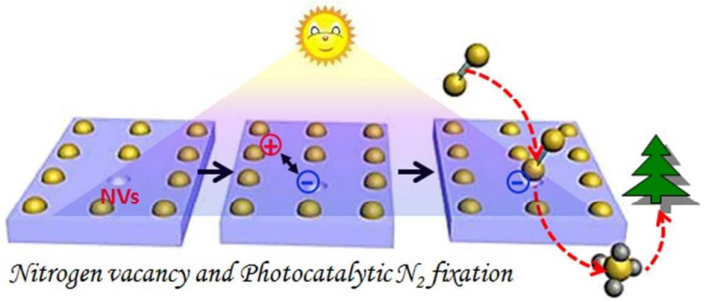

We report for the first time that NV-incorporated g-C_3N_4 can selectively photoreduce N_2 and free from the interference of other gases.